inorganics

MDPI

Article

Mechanochemical Induced Structure Transformations in Lithium Titanates: A Detailed PXRD and ^{6}Li MAS NMR Study

Dennis Becker, Robert Haberkorn and Guido Kickelbick *

Inorganic Solid State Chemistry, Saarland University, Campus, Building C 4 1, 66123 Saarbrücken, Germany; dennis.becker@uni-saarland.de (D.B.); haberkorn@mx.uni-saarland.de (R.H.)

* Correspondence: guido.kickelbick@uni-saarland.de; Tel.: +49-681-302-70651

Received: 30 September 2018; Accepted: 23 October 2018; Published: 27 October 2018

Abstract: Lithium titanates are used in various applications, such as anode materials for lithium intercalation ($Li_4Ti_5O_{12}$) or breeding materials in fusion reactors (Li_2TiO_3). Here, we report the formation of nano-crystalline lithium titanates by a mechanochemical approach and present a deeper insight into their structural characteristics by X-ray diffraction (XRD) and solid-state NMR spectroscopy. The compounds were synthesized in a high-energy planetary ball mill with varying milling parameters and different grinding tools. NaCl type Li_2TiO_3 (α-Li_2TiO_3) was formed by dry milling of lithium hydroxide with titania (rutile or anatase) and by a milling induced structure transformation of monoclinic β-Li_2TiO_3 or spinel type $Li_4Ti_5O_{12}$. Heating of mechanochemical prepared α-Li_2TiO_3 induces a phase transformation to the monoclinic phase similar to hydrothermal reaction products, but a higher thermal stability was observed for the mechanochemical formed product. Microstructure and crystallographic structure were characterized by XRD via Rietveld analysis. Detailed phase analysis shows the formation of the cubic phase from the various educts. A set of two lattice parameters for α-Li_2TiO_3 was refined, depending on the presence of OH^- during the milling process. An average crystallite size of less than 15 nm was observed for the mechanochemical generated products. The local Li environment detected by ^{6}Li NMR revealed Li defects in the form of tetrahedral instead of octahedral site occupation. Subsequent adjustment of the structural model for Rietveld refinement leads to better fits, supporting this interpretation.

Keywords: lithium titanium oxide; mechanochemistry; high energy ball milling; X-ray diffraction; Rietveld refinement; ^{6}Li SPE MAS NMR; impedance spectroscopy

1. Introduction

High energy ball milling (*hebm*) is a versatile tool in the synthesis of metal oxides [1]. Beside the formation of oxide phases that can also be produced in other solid-state reactions, such as high temperature or hydrothermal reactions, it is possible to obtain nanocrystalline high-temperature or high-pressure phases, which are not accessible with traditional synthetic techniques. Examples are the formation of a high-pressure polymorph of TiO_2 starting from anatase or the formation of a $(Zr_{1-x}Ti_x)O_2$ solid solution [2,3]. The milling process can also be used for a solvent-free surface functionalization of nanocrystallites due to the formation of reactive surfaces during the milling process [4]. Additionally, milling generates defects in the form of oxygen vacancies in anatase, as shown by impedance spectroscopy measurements [5].

Li_2TiO_3 represents an interesting system for high energy ball milling because of the three known polymorphs that might be converted under the milling conditions depending on the energy impact. The monoclinic low temperature modification β-Li_2TiO_3 (Figure 1a) with space group $C2/c$ has a

layered structure with three different lithium sites and two different titanium sites and is isostructural to Li_2SnO_3 [6–9]. The cubic high temperature modification γ-Li_2TiO_3 (Figure 1b) with space group *Fm*−3*m* consists of a NaCl type structure with statistical distribution of Li^+ and Ti^{4+} on the 4*a* site and *Z* = 4/3 formula units per unit cell ($Li_{2.66}Ti_{1.33}O_4$) [7–9]. The β polymorph undergoes a reversible transformation to the γ polymorph at approximately 1150 °C [7,10]. A metastable cubic low temperature form with space group *Fm*−3*m* is obtained by hydrothermal reactions from LiOH and TiO_2 in water and is denoted as α-Li_2TiO_3 [7,11–13]. An irreversible phase transformation from hydrothermally formed α-Li_2TiO_3 to β-Li_2TiO_3 occurs after heating above 300 °C [13–15].

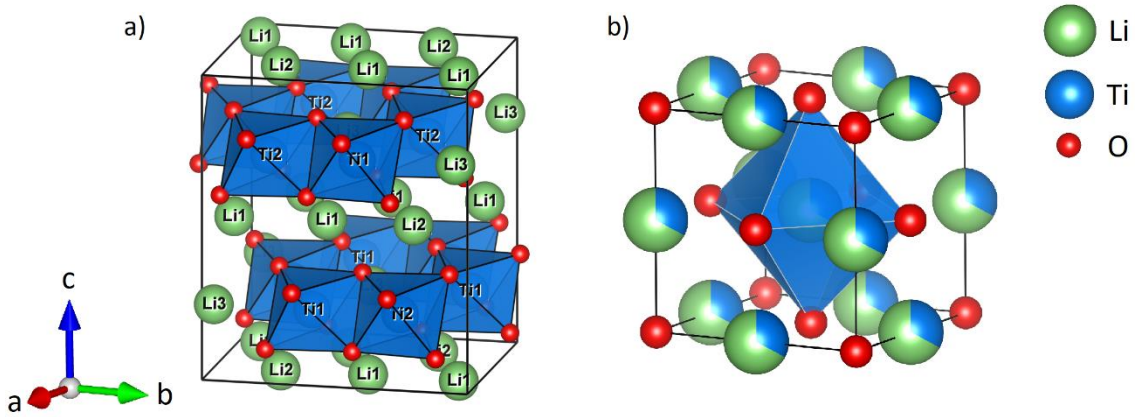

Figure 1. Unit cell of monoclinic β-Li_2TiO_3 (**a**) and cubic α/γ-Li_2TiO_3 (**b**). The green spheres represent lithium, blue titanium and red oxygen. Only polyhedra around titanium (**a**) or a single octahedra (**b**) are shown, to emphasize the structural features.

Ball milling of monoclinic β-Li_2TiO_3 enhances the long-range ion transport, while also inducing a partial transformation to the cubic α polymorph and amorphization, but neither quantitative conversion nor details of the structural properties or phase compositions after milling have been reported yet [16]. The α polymorph may also be obtained by milling of NaOH, LiCl and TiO_2, but subsequent washing to remove NaCl is necessary and no structural characterization of the product is given [17]. For $Li_4Ti_5O_{12}$, a well-known Li-ion battery anode material, an increase in ion conductivity is reported after milling, but no structure transformation or structural changes by milling have been reported in the literature yet [18].

The goal of our study was the investigation of mechanochemical-induced processes in lithium titanates and the systematic study of process parameters such as milling tools, milling times and milling speed via detailed powder X-ray diffraction (PXRD) Rietveld refinement and ^{6}Li single pulse excitation magic angle spinning NMR (SPE MAS NMR) experiments. The mechanochemical induced synthesis of cubic α-Li_2TiO_3 from the simple educts LiOH and TiO_2 is reported for the first time and its thermal stability is explored by PXRD. Furthermore, the mechanochemical induced phase transformation of β- to α-Li_2TiO_3 is examined by PXRD and additionally by ^{6}Li NMR experiments, revealing occupation of tetrahedral sites by lithium. Subsequent modification of the structural model for α-Li_2TiO_3 improves the Rietveld refinement. Lastly, PXRD and ^{6}Li NMR experiments reveal a strong structural influence on spinel $Li_4Ti_5O_{12}$ by mechanochemical treatment.

2. Results and Discussion

2.1. Mechanochemical Formation of α-Li_2TiO_3 from LiOH and TiO_2

High energy ball milling of LiOH with rutile or anatase as titania precursors in yttrium stabilized zirconia (ZrO_2) and tungsten carbide/cobalt hard metal (WC) tools leads to the formation of new reflections in the X-ray diffractogram which may be indexed by a cubic unit cell, as already noted in a previous study [19]. The new reflections could be assigned to either $LiTiO_2$ or Li_2TiO_3 with NaCl type

structure (SG *Fm*−3*m*) and a refined lattice parameter *a* varying between 4.15 and 4.16 Å, depending on the reaction conditions. While both compounds have the same structure type, a quantitative reduction of Ti^{4+} to Ti^{3+} is required to form $LiTiO_2$. This is unlikely under the given conditions, since a reducing agent or oxygen release would be necessary. However, the appearance of very small portions of Ti^{3+} in TiO_2 has been described as a result of defect formation by mechanochemical methods [20]. The mechanochemical formation of $LiTiO_2$ has been described before by milling of Li_2O, TiO_2 and Ti, with larger impurities of elemental iron from abrasion of the steel milling tools [21]. Furthermore, $LiTiO_2$ is black in color [22], while the products of our process are white if ZrO_2 tools are used or gray if WC tools are used. The grey color is based upon abrasion from the WC tools [23]. Hence, the composition of the milling products corresponds to a composition close to Li_2TiO_3 with a mean Ti oxidation state of nearly IV. Due to the additional anatase to high pressure phase transformation [2], milling products of LiOH and anatase show a complex phase composition. The Rietveld refinement of the milling product from ZrO_2 tools after 6 h of milling at 600 rpm is shown as an example in the Supplementary Materials (Figure S1). The reflections of the high-pressure polymorph TiO_2-II overlap with the reflections of anatase and α-Li_2TiO_3. Additionally, milling with anatase as the titania precursor leads to a smaller portion of cubic phase after the same milling conditions.

Based on the reported results we decided to only discuss the rutile ball milling more closely in the following sections. PXRD measurements of LiOH, rutile and the milling products with different parameters are shown in Figure 2. Decrease of the TiO_2 main reflection and rise of new α-Li_2TiO_3 reflections are marked by yellow rectangles. Formation of Li_2CO_3 (marked by triangles) is caused by unreacted amorphous LiOH which forms crystalline Li_2CO_3 on contact with air, allowing for quantification by Rietveld refinement.

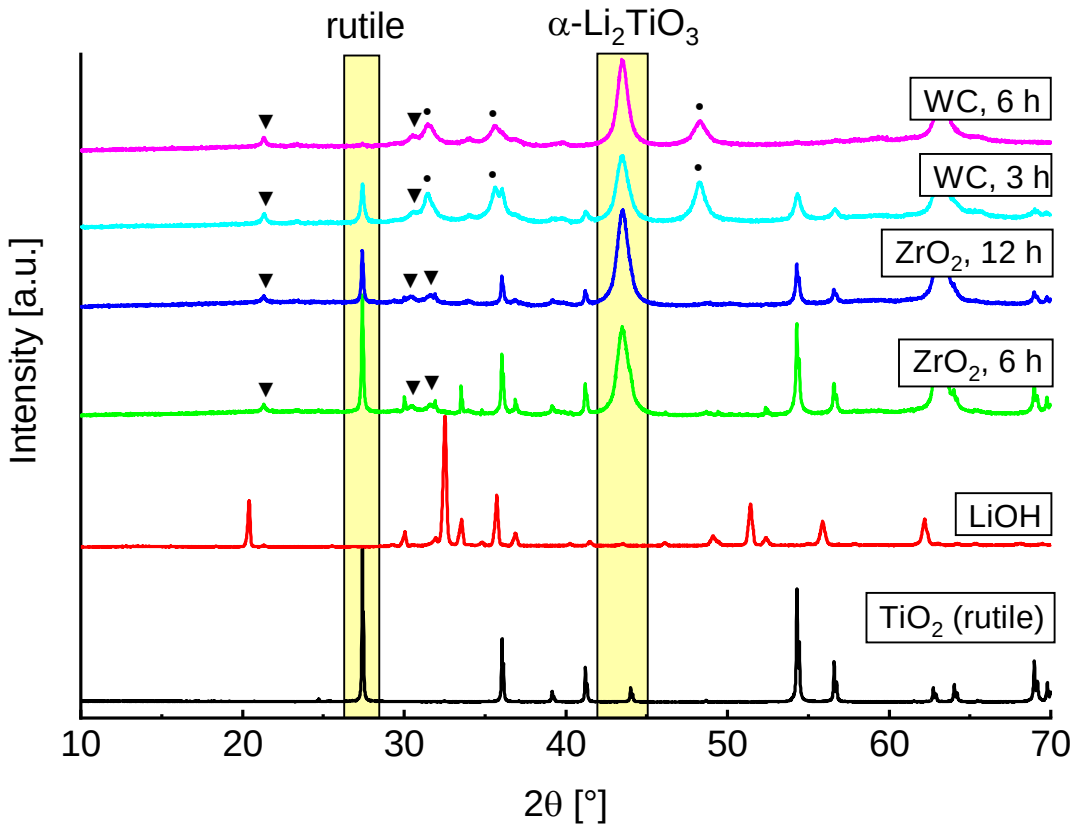

Figure 2. PXRD measurements of LiOH and rutile after different milling conditions. Excess LiOH forms Li_2CO_3 after the milling process (triangles). WC reflections (circles) arise due to abrasion of the tools.

A faster formation of α-Li_2TiO_3 can be observed by use of WC milling tools. Rietveld refinements indicate an introduction of 2 to 4% crystalline WC from abrasion of the tools (marked by circles). After a milling time of 6 h no rutile reflections are visible, while these are still present after 12 h if ZrO_2 tools are used. This is most likely due to the different hardness of the milling tools and the resulting variations in impact energies. There are already reports in the literature which indicate that the milling tools can have a large influence on the formation of different phases [3,24].

Only results obtained by using WC tools are discussed more closely in the following, since they show a more efficient conversion to cubic Li_2TiO_3. Depending on the milling parameters, the refined structural parameters of the PXRD measurements are slightly different. The lattice parameter *a* varies and the crystallite size is in the range of 10 to 15 nm. Since OH^- anions are readily available by using LiOH in the mechanochemical synthesis, substitution of O^{2-} by OH^- may be the case to some extent, resulting in a variation of the lattice parameter (4.15–4.16 Å) depending on the degree of substitution. Because only traces of H_2O were found during TG-IR investigation (Supplementary Materials Figures S4 and S5) only a small amount of OH^- may be assumed but different OH^- contents caused by varying conditions of synthesis account for the different lattice parameters of the as prepared products.

Higher amounts of cubic Li_2TiO_3 were only obtained after long milling times or high milling speeds (Figure 3). The cubic phase formed slowly at lower rotational speeds (400 rpm) and even after 24 h a portion of 50% was not exceeded. At high milling speeds (600 rpm) a portion larger than 50% was already achieved after milling for only three hours.

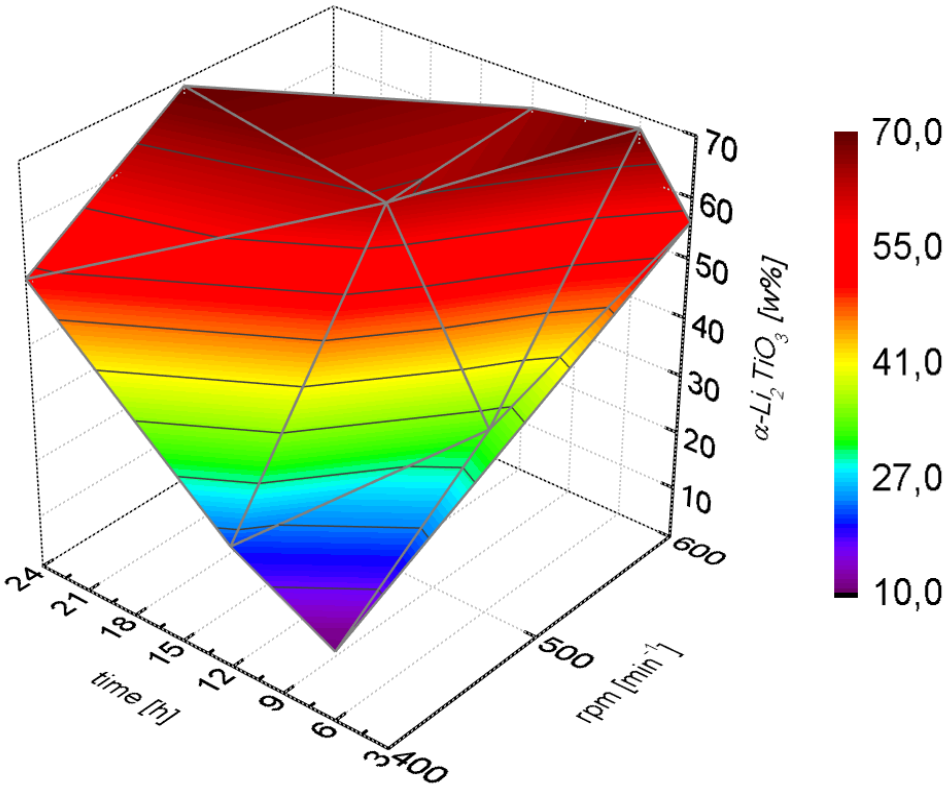

Figure 3. Weight portions (from Rietveld refinement) of α-Li_2TiO_3 after milling of LiOH and rutile in WC tools with different parameters.

The percentage of α-Li_2TiO_3 after milling at 600 rpm for 6 h amounts to 68%, as analyzed by Rietveld refinement (Figure 4) neglecting possibly existing amorphous matter. Since Li_2CO_3 is still present after complete conversion of TiO_2 and an increased baseline intensity is visible, a portion of amorphous material may be assumed. Handling of the milling product in a glovebox with subsequent measurement in an airtight dome sample holder (Rietveld refinement in Supplementary Materials

Figure S2) reveals no crystalline phase of LiOH nor Li_2CO_3, therefore Li_2CO_3 is formed after the milling process from the amorphous material by exposure to air. Measurements with an internal standard (50% of α-Al_2O_3) led to the identification of approximately 35% amorphous content, which may contain missing amounts of TiO_2.

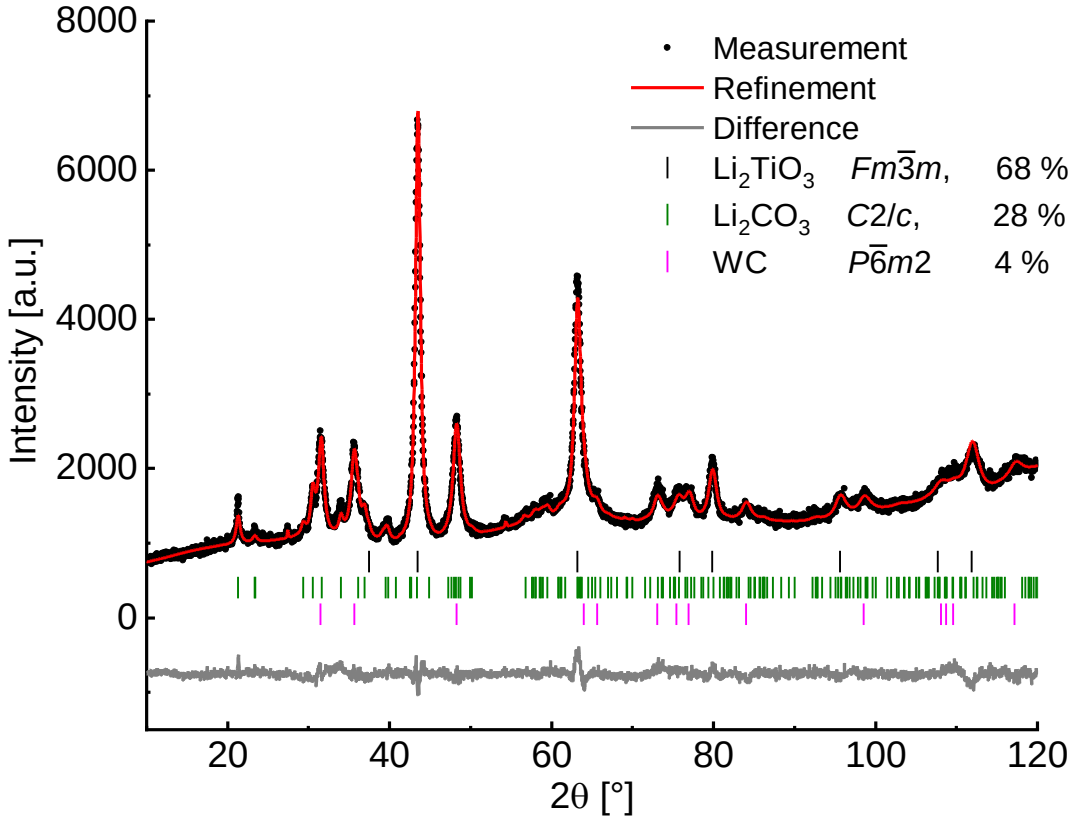

Figure 4. Rietveld plot of the milling product from LiOH and rutile (WC tools, 600 rpm, 6h). Li_2TiO_3 in SG *Fm*−3*m* with a = 4.1588(2) Å, V = 71.93(1) Å^3, number of reflections = 8 and R_{Bragg} = 1.17%. Refinement parameters: number of independent parameters = 40, R_{wp} = 3.44%, R_{exp} = 2.60%, GOF = 1.32. For more detailed refinement parameters see Supplementary Materials Table S1.

If the amorphous content is assumed to contain the starting composition, the total formula may be written as $Li_{2-4x}Ti_{1+x}O_3$ to consider a non-stoichiometry. A formula of $Li_{1.4}Ti_{1.15}O_3$ (x = 0.15) is necessary to stay in the range of the starting composition with a Li to Ti ratio of 2:1. A constrained refinement of the Li and Ti occupancy on the *4a* site of α-Li_2TiO_3 also suggests a lithium deficiency. However, to preserve electric neutrality one titanium substitutes four lithium atoms resulting in a small electronic contrast and, accordingly, these refinements rather represent a general tendency and no absolute values. Since Li_2CO_3 crystallized only after the reaction, the remaining amorphous content may be assumed to be only or mainly TiO_2 in which case a nearly stoichiometric compound with the formula Li_2TiO_3 would be obtained. Thermogravimetric analysis reveals a mass loss of 16.2% (Supplementary Materials, Figure S4) upon heating to 1000 °C. IR coupling of the gas flow shows primarily characteristic bands of carbon dioxide besides traces of H_2O (Supplementary Materials, Figure S5), indicating crystalline Li_2CO_3 as the main fraction responsible for the mass loss. Therefore, the amorphous background is assumed to be primarily TiO_2.

SEM images (Supplementary Materials, Figure S3) indicate that large agglomerates with a seemingly granular surface were formed in the milling process. The primary grains of the agglomerates that form the surface are visible. The grain size of the primary grains is in the range of 20 nm and is of the same order as the refined crystallite sizes.

2.2. Thermal Transformation of α-Li_2TiO_3 to β-Li_2TiO_3

The thermal stability of mechanochemical formed α-Li_2TiO_3 (milling of LiOH and rutile in WC tools at 600 rpm for 6 h) was investigated by successive heating in 100 K steps for 1 h and subsequent PXRD measurement at ambient conditions after each step (Figure 5). Between 300 and 500 °C, the formation of a broad reflection in the range around 20° 2θ indicates a short-range ordering phenomenon. Since the range in which the reflection is formed coincides with the position of the 002-reflection (18.5°) of β-Li_2TiO_3, the broad reflection is probably caused by the nucleation of the monoclinic phase. Sharp reflections of β-Li_2TiO_3 become evident between 500 and 600 °C. The transformation is completed at temperatures over 700 °C. Compared to the hydrothermal synthesis of α-Li_2TiO_3, sharp reflections of β-Li_2TiO_3 are visible at 420 °C and the transformation is nearly complete at 500 °C, with only minor amounts of the α-phase visible (estimated at 12%) [14].

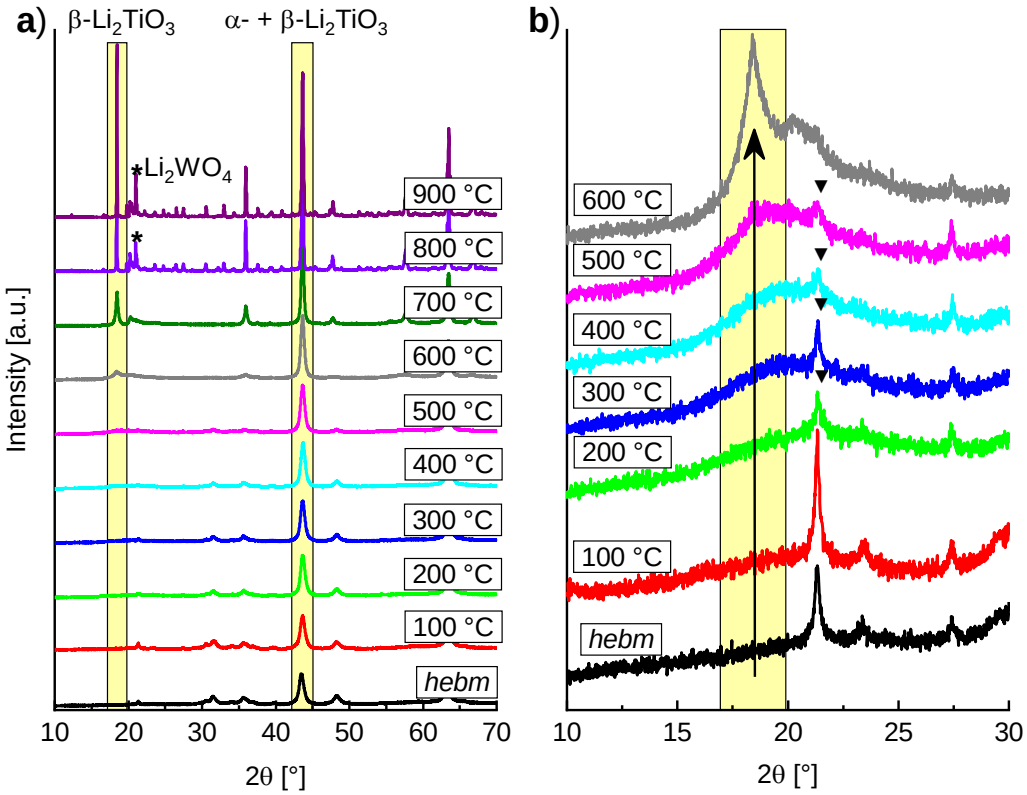

Figure 5. PXRD measurements of high energy ball milling (*hebm*) Li_2TiO_3 after heating to different temperatures for 1 h. (**a**) Main reflections of β- and α-Li_2TiO_3 are highlighted; (**b**) The arrow indicates the deployment of the (002) reflection of β-Li_2TiO_3 between 500 and 600 °C. Triangles indicate the main reflection of Li_2CO_3.

The lattice parameter *a* of α-Li_2TiO_3 changes from 4.1588(2) to 4.1435(1) Å after heating to 200 °C for 1 h. This may be a consequence of the previously mentioned hypothetical OH^- contents in the lattice of an as-prepared α-Li_2TiO_3. Heating induces a transformation of OH^- to O^{2-} and H_2O, leaving the cubic phase with a smaller lattice parameter. Additionally, a high phase portion of α-Li_2TiO_3 has been obtained under these mild conditions, with only 7% Li_2CO_3 remaining and without affecting crystallite size of the cubic phase (Rietveld refinement shown in Supplementary Materials, Figure S6).

In the temperature range between 300 °C and 600 °C, a single fraction of β-Li_2TiO_3 was used in the refinements to estimate the proportion of cubic and monoclinic Li_2TiO_3. Starting with a temperature of 600 °C a three-fraction model for β-Li_2TiO_3 was used (described under Section 3.4). Increasing amounts of 30 to 90% monoclinic fraction were refined in the temperature range between 300 and 700 °C, while the amount of α-Li_2TiO_3 was decreasing. However, up to 500 °C the intensities

of the cubic reflections are hardly affected. This either indicates that the monoclinic ordering arises from byproducts without affecting the cubic structure, or that the ordering takes place continuously. The refined phase portions of α-Li_2TiO_3 (cubic) Li_2CO_3 and β-Li_2TiO_3 (monoclinic) are depicted in Figure 6 with the corresponding calcination temperature.

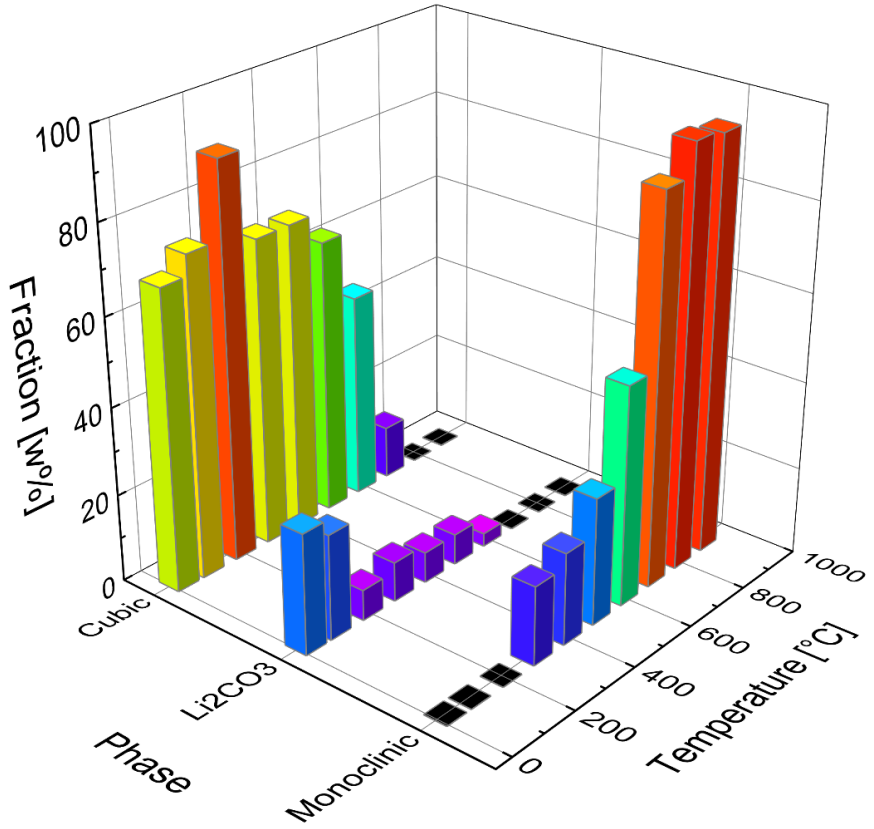

Figure 6. Graphical representation of the refined phase portions of α-Li_2TiO_3, (cubic) Li_2CO_3 and β-Li_2TiO_3 (monoclinic) and the corresponding calcination temperature.

Thermogravimetric analysis (Supplementary Materials, Figure S4) between 25 and 1000 °C shows a mass loss up to the temperature range of 575 to 600 °C (attributed to Li_2CO_3). An exothermic signal arises in the calculated differential thermal analysis (DTA) curve, which correlates to the complete crystallization of β-Li_2TiO_3 as observed in the PXRD measurements. At 600 °C a composition with equal amounts of α- and β-Li_2TiO_3 was refined. Fitting with only the monoclinic phase led to an insufficient refinement (*GOF* = 4.39) while inclusion of the cubic phase results in a greatly improved description (*GOF* = 1.42). At 700 °C an abrupt increase to >90% β-Li_2TiO_3 occurs, with only minor amounts of the cubic phase remaining. Fitting with only the monoclinic structure results in a similar description (*GOF* = 2.09) as by using both structures (*GOF* = 1.93). Though the improvement of the description is small, this may still be attributed to remaining portions of the cubic phase. This leads to an overall interpretation that an ordering phenomenon takes place in the cubic phase at lower temperatures with a discrete structure change between 600 and 700 °C.

2.3. Mechanochemical Induced Phase Transformation of β-Li_2TiO_3 and Spinel $Li_4Ti_5O_{12}$ to α-Li_2TiO_3

The ball milling-induced phase transformation from β- to α-Li_2TiO_3 has already been mentioned by Brandstätter et al. [16], but no further investigation in terms of a quantitative conversion was conducted. In Figure 7, PXRD measurements of β-Li_2TiO_3 before and after milling with (a) ZrO_2 tools and (b) WC tools at different parameters are shown. In both cases (a) and (b), a decrease of the β-Li_2TiO_3 main reflection can be seen. Milling with ZrO_2 tools at 600 rpm for 6 h leads to portions

of 48% α-Li_2TiO_3, 25% β-Li_2TiO_3 and 28% Li_2CO_3. Prolonged milling leads to a further increase in intensity of Li_2CO_3 reflections. In contrast, the ball milling induced phase transformation is already detectable after milling for 10 min in WC tools. A portion of ca. 30% α-Li_2TiO_3 can be fitted, with small amounts of Li_2CO_3 (<10%). Even after milling for 1 h, only marginal amounts of ca. 5% β-Li_2TiO_3 remained. Milling with WC tools leads to complete disappearance of β-Li_2TiO_3 reflections after 6 h. Portions of 89% α-Li_2TiO_3, 8% Li_2CO_3 and 3% WC have been refined (Rietveld refinement in Supplementary Materials, Figure S7). Similar to the mechanochemical synthesis from LiOH and rutile, an increase in baseline intensity suggests the formation of amorphous material. Refinement of β-Li_2TiO_3 (milling in WC tools for 6 h) with an internal standard (50% of α-Al_2O_3) suggests a portion of 27% amorphous background. In comparison to the mechanochemical synthesis from LiOH and rutile in WC tools, a smaller lattice parameter a = 4.1463(2) Å is refined for α-Li_2TiO_3 if β-Li_2TiO_3 is used as an educt. This may also be a consequence of the previously mentioned hypothetical OH^- contents in the lattice. Since no OH^- is available in the mechanochemical-induced phase transformation of β- to α-Li_2TiO_3, a lattice parameter similar to the one of α-Li_2TiO_3 after heating to 200 °C is refined.

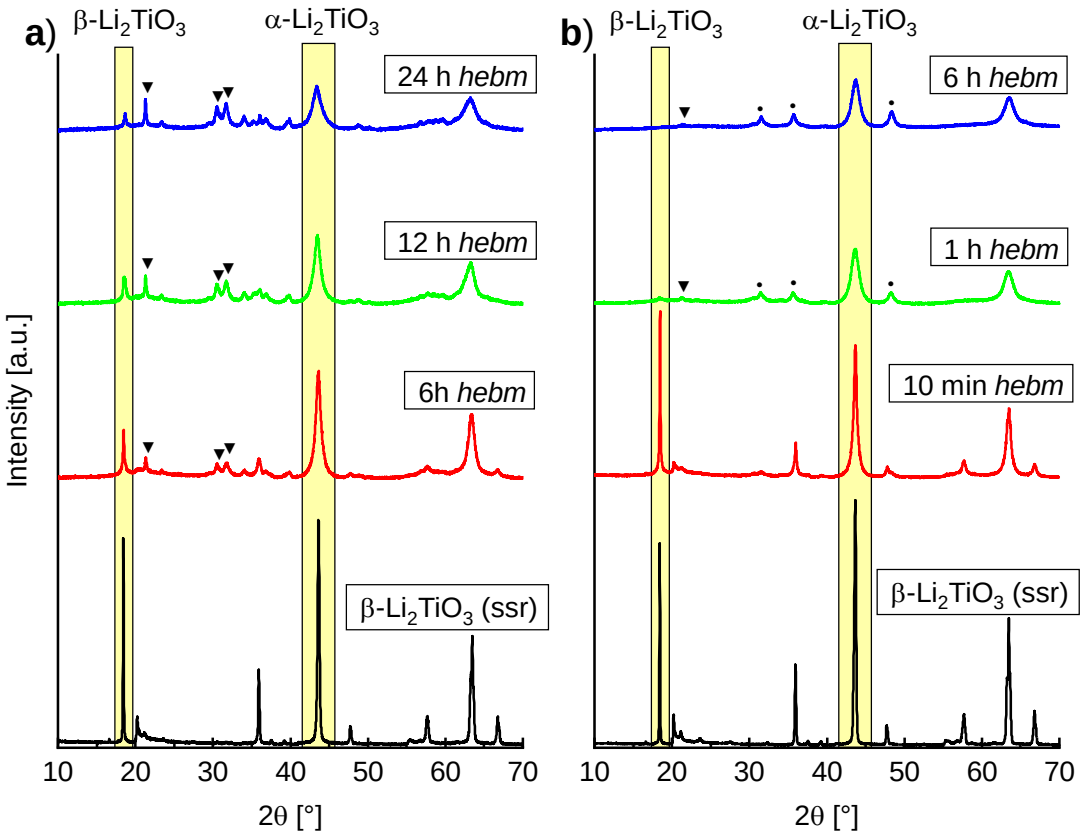

Figure 7. PXRD measurements of β-Li_2TiO_3 after milling in (**a**) ZrO_2 and (**b**) WC tools at 600 rpm after different grinding times. Triangles indicate Li_2CO_3, circles indicate WC.

Formation of α-Li_2TiO_3 is also observed by milling of $Li_4Ti_5O_{12}$ with spinel type structure. PXRD measurements of $Li_4Ti_5O_{12}$ before and after milling in WC tools at 400 rpm are shown in Figure 8a. After a milling time of 1 h a slight asymmetric broadening of the (400) reflection is visible, while the (111) reflection is not as strongly affected and shows little asymmetry. This is caused by the formation of α-Li_2TiO_3 whose reflections overlap with the spinel reflections. In Figure 8b the Bragg intensities of the spinel (400) and the α-Li_2TiO_3 (200) reflection are shown with the resulting Rietveld fit. The (111) reflection of the spinel phase vanishes completely after a milling time of 6 h. Though a phase with cubic structure is formed, the intensities are very low and additional unidentified reflections are visible. Even after these mild milling conditions, the structure of the spinel phase is

strongly altered, which may have large impact on the use of mechanochemically treated $Li_4Ti_5O_{12}$ as anode material in battery applications. It has already been established by impedance spectroscopy that milling of $Li_4Ti_5O_{12}$ leads to an increase in conductivity [18]. This may be due to this partial structure transformation of spinel $Li_4Ti_5O_{12}$ to α-Li_2TiO_3.

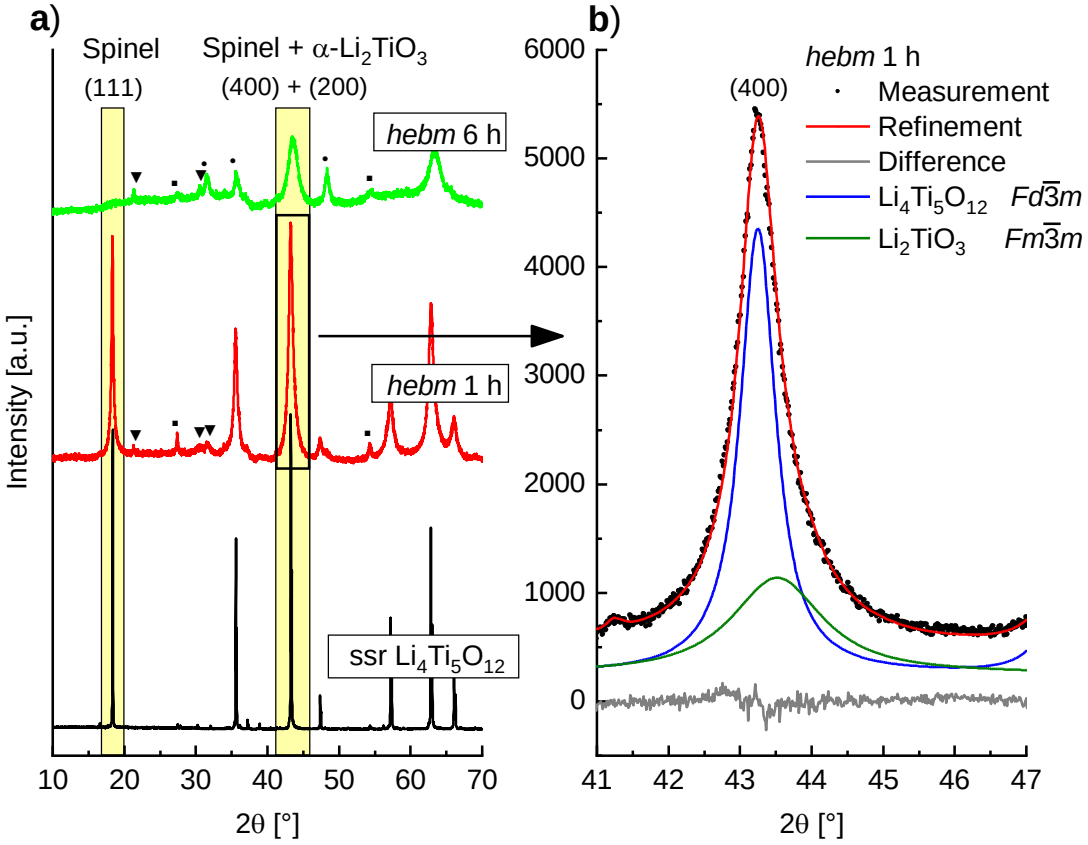

Figure 8. (**a**) PXRD of spinel $Li_4Ti_5O_{12}$ before and after milling in WC tools at 400 rpm for 1 h and 6 h. Data of $Li_4Ti_5O_{12}$ were scaled by a factor of 0.5. Triangles indicate Li_2CO_3, squares indicate rutile and circles indicate WC reflections; (**b**) Enhanced section of the Rietveld plot after milling for 1 h, with fitted portions of spinel (blue) and NaCl type structure (green).

2.4. ^{6}Li SPE MAS NMR

^{6}Li SPE MAS NMR experiments reveal additional insight into the milling-induced structure transformation. To illustrate the following interpretations, the unit cell of spinel $Li_4Ti_5O_{12}$ is shown in Figure 9. (The unit cell of monoclinic β-Li_2TiO_3 is shown in Figure 1.)

PXRD refinements of 900 °C sintered β-Li_2TiO_3 with constrained lithium site occupancy factors (total Li content is 2.0 Li per formula unit) show a full occupation of the 8*f* and 4*d* site (Li1 and Li2), while the 4*e* lithium site (Li3) and the two titanium 4*e* sites (Ti1 and Ti2) show a mixed occupation with 0.6 Li on the Li3 site, 0.3 Li on the Ti1 site and 0.1 Li on the Ti2 site. To obtain a sample with low Li3/Ti1/Ti2 anti-site mixing, several sintering steps at 1100 °C were necessary. A mixing of 0.1 Li on the Ti1 site and 0.1 Li on the Ti2 site remained.

The ^{6}Li NMR spectrum of 1100 °C sintered β-Li_2TiO_3 is shown in Figure 10a where three signals are visible. Fitting of the line profile was performed with three independent Voigt functions, resulting in shifts of δ = 1.30, 0.80 and 0.23 ppm. The peak at 0.80 ppm is attributed to lithium on the 4*e* site (Li3) in the $LiTi_2$ layer, the peak at 0.23 ppm originates from the two magnetically equivalent lithium sites 8*f* (Li1) and 4*d* (Li2) in the Li_2 layer [25,26]. The signals are consistent with values reported in the literature if an offset of ca. −1 ppm is considered due to the referencing against solid LiCl [27]. The shift of the third signal matches a tetrahedral coordination of lithium [25]. In Figure 10b the ^{6}Li

spectrum of spinel $Li_4Ti_5O_{12}$ is shown. $Li_4Ti_5O_{12}$ may also be written as $(Li)[Li_{0.33}Ti_{1.66}]O_4$ to illustrate the occupation of 1 Li on the tetrahedral and $^1/_3$ Li on the octahedral position. According to the literature, the peak at 1.32 ppm is attributed to tetrahedrally-coordinated lithium on the 8*a* site, and the smaller peak at 0.96 ppm to octahedrally-coordinated lithium on the 16*d* site [28]. Additionally, the NMR spectrum of Li_2CO_3 reveals the solely tetrahedrally-coordinated lithium in this compound (Figure 10c). A single shift of 1.16 ppm is observed, which is also in accordance with the literature [28]. Since pristine compounds of β-Li_2TiO_3 and spinel $Li_4Ti_5O_{12}$ were yielded by solid state reactions, no Li_2CO_3 may be present (confirmed by PXRD measurements). The third signal of β-Li_2TiO_3 is therefore assigned to lithium on an interstitial position with tetrahedral coordination.

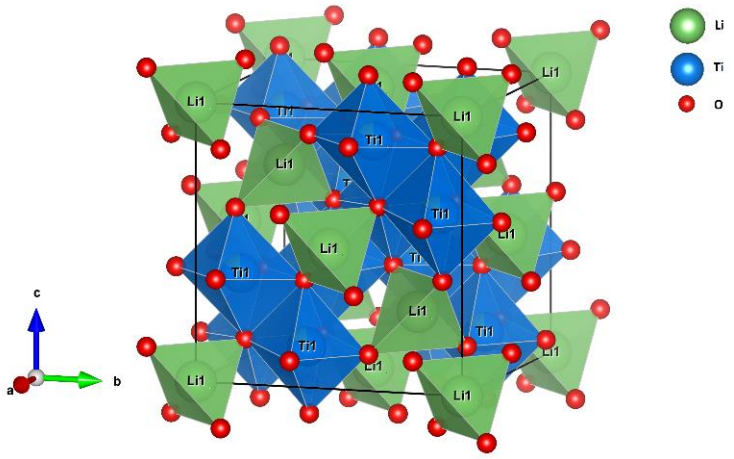

Figure 9. Unit cell of spinel $Li_4Ti_5O_{12}$. The green spheres represent lithium, blue titanium and red oxygen. The Ti1 position inside the octahedra are occupied by 0.833 Ti and 0.167 Li.

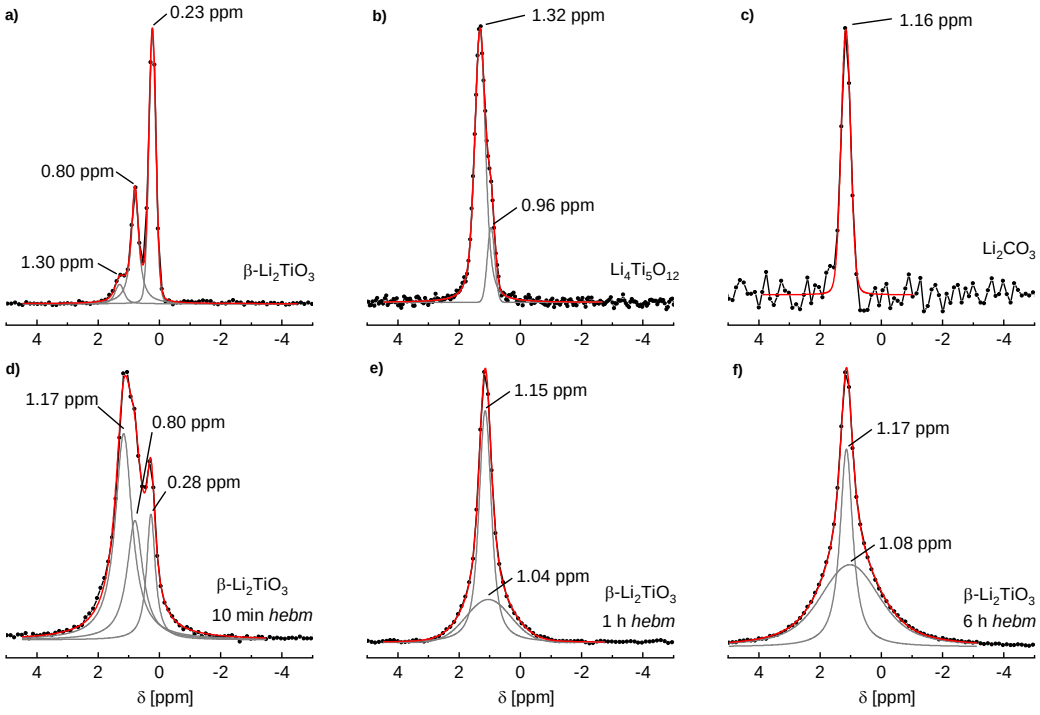

Figure 10. ^{6}Li SPE MAS NMR spectra of (**a**) β-Li_2TiO_3; (**b**) spinel $Li_4Ti_5O_{12}$; (**c**) Li_2CO_3; (**d**) β-Li_2TiO_3 after *hebm* for 10 min; (**e**) 1 h and (**f**) 6 h. All spectra were referenced against solid LiCl and fitted with one, two or three independent Voigt functions with $R^2 > 0.99$.

The spectrum of β-Li_2TiO_3 after 10 min of milling is shown in Figure 10d. The signal formerly at δ = 1.30 ppm is shifted to 1.17 ppm, while the positions of the two other signals are hardly affected. Additionally, the signal intensities of β-Li_2TiO_3 are strongly altered. The signal at 1.17 ppm indicates that more than half the lithium atoms are tetrahedrally coordinated, while only few remain in octahedral coordination. After 1 h of milling (Figure 10e) only two signals are present. The tetrahedral coordination remains as the dominant state indicated by the sharp line at 1.15 ppm. The band at 1.04 ppm, probably caused by cubic Li_2TiO_3 with Li and Ti in octahedral coordination and random ordering, indicates an additional new coordination environment. The signal at 1.15 ppm may be caused by Li_2CO_3 that is formed after the milling process. However, PXRD refinements show a portion of only 19% Li_2CO_3 after milling for 1 h, while the NMR signal is clearly caused by the main fraction in the sample. The tetrahedral coordination in Li_2TiO_3 is therefore assumed to be a transition state for the formation of the cubic state. This new broad signal at ca. 1 ppm becomes the dominant state after milling for 6 h (Figure 10f). The ^{6}Li SPE MAS NMR spectrum of Li_2TiO_3 from milling of LiOH and rutile (WC tools, 6 h milling time) is nearly identical (not shown). This underlines the assumption that this broad signal is caused by octahedrally-coordinated Li in the cubic phase. Parts of the tetrahedra signal remain. This is most probably caused by occupation of interstitial positions and by Li_2CO_3, but it was not possible to separate the contributions of these two states.

The ^{6}Li SPE MAS NMR spectra of $Li_4Ti_5O_{12}$ (Supplementary Materials, Figure S8) show a slightly different behavior compared to the transformation of β-Li_2TiO_3. A broad signal at δ = 1.15 ppm is visible after milling for 1 h, indicating a purely tetrahedral coordination environment. No signal of an octahedral coordination at ca. 1 ppm is visible. Additionally, a small signal at 1.57 ppm can be distinguished. This signal indicates a very short Li-O bonding distance or a coordination number lower than four. This signal may either be attributed to an interstitial position or the unidentified phase seen in PXRD, but no further identification was possible.

In conclusion to the finding that a tetrahedral coordination environment plays a major role in the structure after mechanochemical treatment, a revised structure model for the Rietveld refinement of α-Li_2TiO_3 was constructed. In the ideal NaCl structure model the octahedral 4*a* site is occupied by 1/3 Ti and 2/3 Li (model A). In the revised model, the tetrahedral 8*c* site was added and the corresponding site occupancy factors (*sof*) of Li on the 4*a* site (Li_O) and 8*c* site (Li_T) were refined. To keep the overall stoichiometry of Li_2TiO_3, a constraint refinement in the form [*sof*(Li_T) = $^1/_3$ − $\frac{1}{2}$·*sof*(Li_O)] was defined, while the occupation of Ti was kept constant (model B). The resulting structure parameters are shown in Table 1.

Table 1. Structure model for the Rietveld refinement of α-Li_2TiO_3 with a mixed Li occupation in octahedral and tetrahedral gaps. Li_T = tetrahedra gap, Li_O = octahedra gap, *WP* = Wyckoff position, *sof* = site occupancy factor.

Site	*WP*	x	y	z	Atom	*sof*
Li_T	8*c*	1/4	1/4	1/4	Li^+	0.07(1)
Li_O	4*a*	0	0	0	Li^+	0.53(1)
	4*a*	-	-	-	Ti^{4+}	0.333
O1	4*b*	1/2	1/2	1/2	O^{2-}	1

As a consequence of this adapted model, the Rietveld refinement of milled β-Li_2TiO_3 (WC tools, 600 rpm, 6h) is improved. This can be seen particularly in the description of the 022 reflection, which is depicted in Figure 11 with a fit using the (a) standard model A and (b) the adjusted model B. To better accommodate the shape of the amorphous background, a polynomial of 25th degree was used in these both cases, instead of the elsewise-used polynomial of 15th degree. Both the R_{Bragg} value of the Li_2TiO_3 phase and the overall fit are improved in model B. The *GOF* is reduced from 1.13 in model A to 1.11 in model B, which is only slightly better but nonetheless indicating an improvement. Beyond that, the R_{Bragg} value, which only dependents on the agreement between observed and calculated

reflection intensities of the phase, is significantly lowered from 0.60% in model A to 0.28% in model B. However, since Li has a very low X-ray scattering factor the obtained values for the site occupancies in Table 1 are just an indication of an occupation of the tetrahedral site and cannot be regarded as proof. Nevertheless, this model helps to harmonize the results of the Rietveld refinement with the fitted areas of the signals of tetrahedral and octahedral environments in the ^{6}Li SPE MAS NMR spectrum of milled β-Li_2TiO_3 (WC tools, 600 rpm, 6 h). The areas in the ^{6}Li spectrum sum up to a proportion of 0.59 to 1 for tetrahedral- and octahedral-coordinated lithium, which corresponds to 37% tetrahedrally-coordinated lithium. The phase fraction from Rietveld refinement with model A (7% Li_2CO_3, 90% α-Li_2TiO_3 or 10.2 mol % Li_2CO_3 and 88.3 mol % α-Li_2TiO_3) corresponds to only 10% tetrahedrally coordinated lithium, solely arising from Li_2CO_3. This is far below the 37% from the ^{6}Li spectrum. If tetrahedrally-coordinated lithium in α-Li_2TiO_3 from model B (6.2% Li_2CO_3, 91.1% α-Li_2TiO_3 or 9.0 mol % Li_2CO_3 and 89.5 mol % α-Li_2TiO_3) is factored in, a portion of 30% tetrahedrally-coordinated lithium is obtained, which fits the portion of the Li NMR spectrum. Here, a *sof* of 0.07 for Li on the 8*c* site (Li_T) corresponds to 21% of tetrahedrally coordinated lithium in α-Li_2TiO_3.

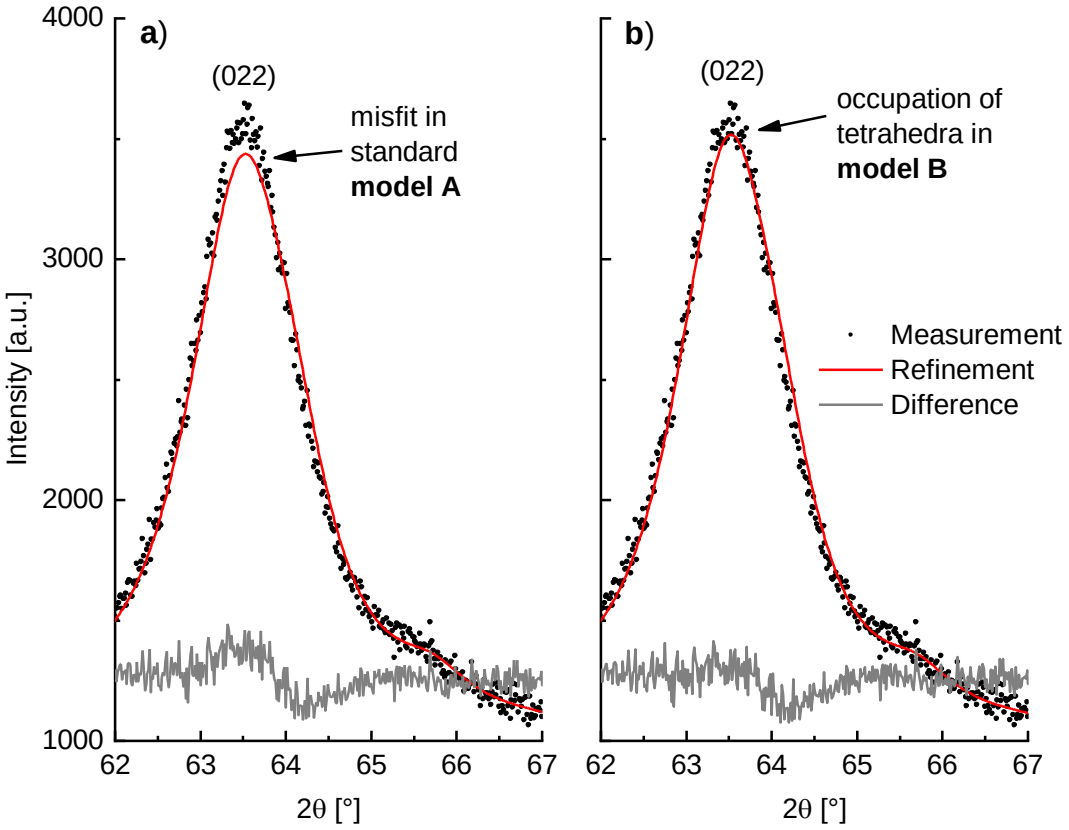

Figure 11. Rietveld refinement of milled β-Li_2TiO_3 (WC tools, 600 rpm, 6 h) with (**a**) the ideal NaCl structure model and (**b**) a NaCl structure with mixed Li occupation in octahedra and tetrahedra gaps. Refinement parameters: (**a**) R_{Bragg} = 0.60%, *GOF* = 1.13 and (**b**) R_{Bragg} = 0.28%, *GOF* = 1.11.

2.5. Impedance Spectroscopy

Since ball milling leads to the formation of defects, structure deformations and amorphization, an influence on the ion conductivity can be expected. The impedance spectra of ball-milled Li_2TiO_3 (600 rpm) and $Li_4Ti_5O_{12}$ (400 rpm) show an increase in conductivity of up to three orders of magnitude. The frequency dependent real part of the conductivity is shown in Figure 12a,b. The spectra were recorded at 298K.

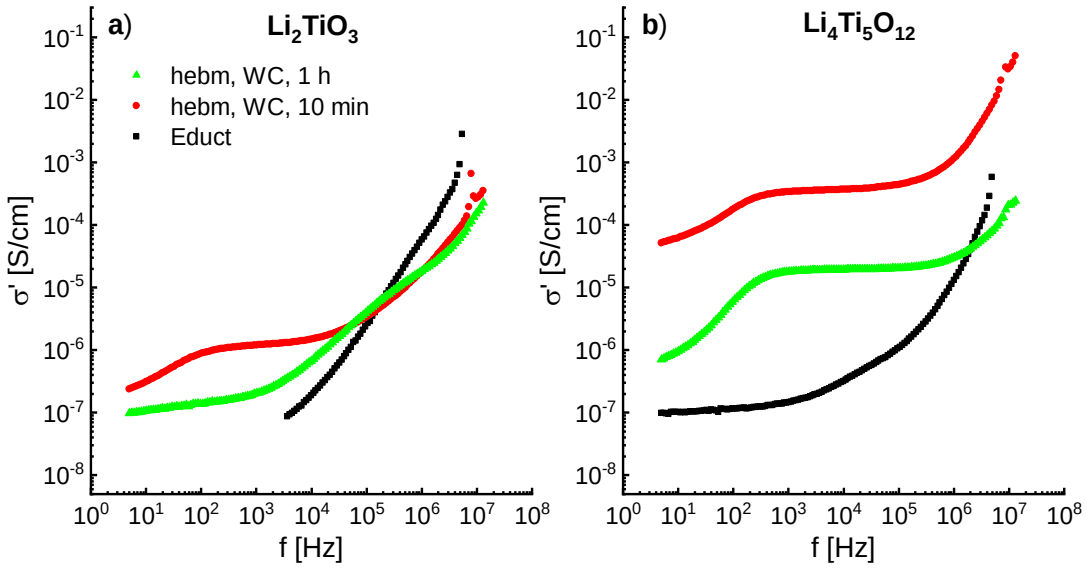

Figure 12. Frequency dependent real part of the conductivity at 298K of (**a**) Li_2TiO_3 and (**b**) $Li_4Ti_5O_{12}$ before and after milling at (**a**) 600 rpm and (**b**) 400 rpm for 10 min and 1 h.

The conductivity of Li_2TiO_3 from the solid-state reaction is rather poor and is immeasurable at frequencies below 3 kHz. After milling for 10 min an increase of one order of magnitude can be observed, with a typical dc plateau ($\sigma_{dc} \approx 10^{-6}$ S/cm) at lower frequencies and a dispersive regime at higher frequencies. Similar results are shown by Brandstätter et al. [16], however, only a conductivity σ_{dc} of about 10^{-9} S/cm is reported at room temperature for a milled sample. Milling of Li_2TiO_3 for 1 h decreases the conductivity to $\approx 10^{-7}$ S/cm, indicating a blocking of the Li ion transport. This may be due to the phase transformation from β- to α-Li_2TiO_3. As already shown by ^{6}Li MAS NMR in Figure 10, milling for 10 min displaces Li to tetrahedrally-coordinated sites, which may be responsible for the increase in conductivity. Longer milling times promote a new octahedral coordinated state, which may be associated to the decrease in conductivity.

$Li_4Ti_5O_{12}$ shows a similar behavior to Li_2TiO_3, with a dc plateau at lower frequencies and a dispersive region at higher frequencies and a decrease of the conductivity after longer milling times. However, $Li_4Ti_5O_{12}$ from solid state reaction already exhibits a dc plateau at lower frequencies with $\sigma_{dc} \approx 10^{-7}$ S/cm at 298 K. Milling for 10 min increases the conductivity by three orders of magnitude to $>10^{-4}$ S/cm at 298 K. The observed conductivities are the highest shown yet for ball-milled $Li_4Ti_5O_{12}$ at room temperature [18].

3. Materials and Methods

3.1. Materials

LiOH (Merck, Darmstadt. Germany, 98%), Li_2CO_3 (Merck, 99%), TiO_2 (Anatase, Merck, ≥99% and Rutile, Alfa Aesar GmbH, Karlsruhe, Germany, 99.5%), 2-propanole (Biesterfeld Spezialchemie, 97%) and *n*-pentane (Sigma Aldrich, Steinheim, Germany, 99%) were used as received. All solids have been characterized by PXRD. The used LiOH contained 20% LiOH·H_2O.

3.2. Sample Preparation

Milling was conducted in a Retsch PM100 planetary ball mill with rotational speeds of 400, 500 and 600 rpm. Milling tools, consisting of yttrium stabilized zirconia (ZrO_2) and tungsten carbide in cobalt matrix (WC) with a volume of 50 mL, as well as 200 milling balls of the same material, with a diameter of 5 mm, were used. The ball to powder weight ratio was 27:1 in case of ZrO_2 and 60:1 in case of WC tools. Approximately 3 g of starting powder ($Li_4Ti_5O_{12}$ or β-Li_2TiO_3) were placed in the

grinding jar. To prevent cementing of the powders, 200 µL of 2-propanole were added as dispersing agent. In case of the mechanochemical synthesis from binary oxides, LiOH and TiO_2 (rutile or anatase) to form 3 g of Li_2TiO_3 were deployed. An excess of 10 mol % LiOH was used.

Spinel $Li_4Ti_5O_{12}$ and β-Li_2TiO_3 were synthesized by conventional solid-state reactions [6,29]. Appropriate amounts of lithium carbonate and anatase were homogenized by wet ball milling with *n*-pentane at 400 rpm for 1 h. A 50-mL agate grinding jar and twenty agate balls of 10 mm diameter were used. The dried mixtures were heated in a platinum crucible to 900 °C for 8 h in air atmosphere. The resulting white powders were manually ground in an agate mortar and reheated a second time. To obtain samples of β-Li_2TiO_3 with higher crystallinity and less Li-Ti-disorder, several heating steps at 1100 °C were carried out.

3.3. Characterization

Powder X-ray diffraction (PXRD) patterns were recorded on a Bruker D8-A25-Advance diffractometer (Bruker, Karlsruhe, Germany) in Bragg–Brentano θ–θ-geometry (goniometer radius 280 mm) with Cu Kα-radiation (λ = 154.0596 pm). A 12 µm Ni foil working as Kβ filter and a variable divergence slit were mounted at the primary beam side. A LYNXEYE detector with 192 channels was used at the secondary beam side. Experiments were carried out in a 2θ range of 7 to 120° with a step size of 0.013° and a total scan time of 2h. Topas 4.2 [30] was used for the Rietveld refinements. Crystallographic structure and microstructure were refined, while instrumental line broadening was included in a fundamental parameters approach [31]. The background was fitted by a Chebychev polynomial function of 15th degree, while fluorescence induced background was reduced by discriminating the detector. Crystal structure data were obtained from the crystallography open database (COD) [32] and inorganic crystal structure database (ICSD).

Thermogravimetric analysis was conducted on a Netzsch TG 209 F1 Iris ASC (Netzsch, Selb, Germany) in alumina crucibles (V = 75 µL), in a temperature range from 25–1000 °C under a nitrogen flow of 40 mL·min^{-1} with a heating rate of 20 K·min^{-1}. The samples were dried in a pre-heating phase at 100 °C under flowing nitrogen and cooled again before the measurement was started. Coupling of the gas flow to a Bruker Vertex 70 IR spectrometer (Bruker, Karlsruhe, Germany) was achieved with a heated transfer line (200 °C) under constant nitrogen flow. Spectra were recorded between 4500 to 600 cm^{-1} with a resolution of 4 cm^{-1} and 32 scans per spectrum.

^{6}Li single-pulse excitation magic angle spinning (SPE MAS) NMR spectra were recorded on a Bruker AV400WB spectrometer (Bruker, Karlsruhe, Germany) (^{6}Li at 58.91 MHz) at 298K in standard ZrO_2 rotors (d = 4 mm). A spinning rate of 12 to 13 kHz and a relaxation delay of 3 s were used. Solid LiCl was used as external reference at 0 ppm.

Impedance spectra were recorded on an HP 4192A impedance analyzer (Hewlett-Packard, Palo Alto, CA, USA) in a frequency range of 5 Hz to 13 MHz at 298 K. Data points were recorded via software [33]. The samples were pressed into pellets with 10 mm diameter and a thickness of 1.4–2.1 mm under a uniaxial pressure of 250 MPa at room temperature. Both sides of the pellets were coated with silver conducting paste and dried overnight in air, to establish electrical contact with the platinum electrodes in the measurement cell.

3.4. Structural Model for β-Li_2TiO_3 in Rietveld Refinement

As already mentioned in the literature, Rietveld refinement of β-Li_2TiO_3 requires a more complex structural model than a single well-ordered phase. A mixed occupancy of Li and Ti in the $LiTi_2$ layer and different stacking variants must be considered to obtain a satisfactory fit [34]. In our work a three-fraction model [35,36] with a Li-Ti-mixing in the $LiTi_2$ layer was used to account for a distribution of different states, but no stacking variants were considered. The parameters of the microstructure of the three fractions were constrained but lattice parameters were refined independently.

4. Conclusions

The cubic polymorph of Li_2TiO_3 was successfully synthesized via high energy ball milling of LiOH with rutile, β-Li_2TiO_3 and spinel $Li_4Ti_5O_{12}$. The material of the used milling tools showed a large impact on the composition of the product powders. Use of tungsten carbide (WC) led to full conversion of rutile with LiOH or β-Li_2TiO_3 to α-Li_2TiO_3. In contrast, the use of yttrium-stabilized zirconia (ZrO_2) did not lead to full conversion, neither of rutile with LiOH nor β-Li_2TiO_3 regardless of the applied milling conditions. TG-IR coupling of the gas flow showed primarily characteristic bands of CO_2, indicating crystalline Li_2CO_3 to be mainly responsible for the mass loss upon heating. Therefore, the amorphous background is assumed to primarily consist of TiO_2.

Heating under mild conditions (200 °C for 1 h) of the mechanically produced cubic phase caused a phase percentage of 90% cubic phase, without affecting the nano-crystallinity. Further heating resulted in an ordering phenomenon with monoclinic structure at lower temperatures, following a discrete structure change between 600 and 700 °C resulting in a full transformation to β-Li_2TiO_3.

Even after mild milling conditions, the structure of spinel $Li_4Ti_5O_{12}$ is strongly altered, which may have a large impact on the use of mechanochemical treated $Li_4Ti_5O_{12}$ as anode material. Though a phase with cubic structure was formed, the reflections were very broad and additional unidentified reflections were visible.

^{6}Li SPE MAS NMR spectra revealed an extensive rearrangement of the Li environment in β-Li_2TiO_3 after 10 min of milling. A tetrahedrally coordinated state may be occupied by Li. NMR spectra of the mechanochemically treated spinel $Li_4Ti_5O_{12}$ indicated a purely tetrahedrally-coordinated environment after milling for 1 h. The process of the milling-induced transformation of the spinel is not completely understood yet. In conclusion to these findings, a revised structure model including a tetrahedral Li site in cubic Li_2TiO_3 was tested in Rietveld refinement and resulted in a slightly improved fit.

Impedance spectroscopy measurements at 298K show an increase in conductivity of up to three orders of magnitude after milling for just 10 min. This may be due to the displacement of Li ions to tetrahedrally-coordinated or interstitial sites (as observed by ^{6}Li NMR). Longer milling times tend to decrease the conductivity again. These results may be a hint of how to activate anode materials for a faster lithium intercalation.

Supplementary Materials: The following are available online at http://www.mdpi.com/2304-6740/6/4/117/s1, Figure S1: Rietveld refinement of the milling product from LiOH and anatase, Figure S2: Rietveld refinement of the milling product from LiOH and rutile, Figure S3: SEM photograph of the milling product from LiOH and rutile, Table S1: Refined structure parameters of α-Li_2TiO_3 produced by milling of LiOH and rutile, Figure S4: TGA and calculated DTA curve of Li_2TiO_3 from milling of LiOH and rutile, Figure S5: Temperature dependent IR signals from coupling of TGA gas flow to IR detector, Figure S6: Rietveld refinement of the milling product from LiOH and rutile, Figure S7: Rietveld refinement of β-Li_2TiO_3 after ball milling with WC tools for 6 h at 600 rpm, Figure S8: ^{6}Li SPE MAS NMR spectra of (a) spinel $Li_4Ti_5O_{12}$; (b) after *hebm* for 1 h.

Author Contributions: Conceptualization, D.B., R.H. and G.K.; Methodology and Formal Analysis, D.B. and R.H.; Investigation, D.B.; Resources, G.K.; Writing—Original Draft Preparation, D.B.; Writing—Review & Editing, D.B., R.H., and G.K.; Visualization, D.B.; Supervision, R.H. and G.K.

Funding: This research received no external funding.

Acknowledgments: We would like to thank Christina Odenwald for recording of the SEM photographs and Michael Zimmer for conducting the NMR experiments and helpful discussion.

Conflicts of Interest: The authors declare no conflict of interest.

References

1. Fuentes, A.F.; Takacs, L. Preparation of Multicomponent Oxides by Mechanochemical Methods. *J. Mater. Sci.* **2013**, *48*, 598–611. [CrossRef]
2. Chaudhuri, J.; Ram, M.L.; Sarkar, B.K. Observation of a High Pressure Polymorph of Titania by Vibrational Ball Milling. *J. Mater. Sci.* **1994**, *29*, 3484–3488. [CrossRef]

3. Kong, L.; Ma, J.; Zhu, W.; Tan, O. Phase Formation and Thermal Stability of $(Zr_{1-x}Ti_x)O_2$ Solid Solution via a High-Energy Ball Milling Process. *J. Alloys Compd.* **2002**, *335*, 290–296. [CrossRef]
4. Fischer, A.; Ney, C.; Kickelbick, G. Synthesis of Surface-Functionalized Titania Particles with Organophosphorus Coupling Agents by Reactive Milling. *Eur. J. Inorg. Chem.* **2013**, *2013*, 5701–5707. [CrossRef]
5. Amade, R.; Heitjans, P.; Indris, S.; Finger, M.; Haeger, A.; Hesse, D. Defect Formation during High-Energy Ball Milling in TiO_2 and Its Relation to the Photocatalytic Activity. *J. Photochem. Photobiol. A Chem.* **2009**, *207*, 231–235. [CrossRef]
6. Lang, G. Die Kristallstruktur Einiger Vertreter Der Verbindungsklasse $Me_2Me^{IV}O_3$ Als Beitrag Zur Aufklärung Der Ordnungsphase von Li_2TiO_3. *J. Inorg. Gen. Chem.* **1954**, *276*, 77–94. [CrossRef]
7. Giquel, C.; Mayer, M.M.; Bouaziz, R.; Champetier, M.G. Sur Quelques Composés Oxygénés Du Titane et Des Alcalins (Li, Na); Étude Des Binaires M_2O-TiO_2 Dans Les Zones Riches En Oxyde Alcalin. *C. R. Acad. Sc. Paris* **1972**, *275*, 1427–1430.
8. Mikkelsen, J.C. Pseudobinary Phase Relations of $Li_2Ti_3O_7$. *J. Am. Ceram. Soc.* **1980**, *63*, 331–335. [CrossRef]
9. Kleykamp, H. Phase Equilibria in the Li–Ti–O System and Physical Properties of Li_2TiO_3. *Fusion Eng. Des.* **2002**, *61–62*, 361–366. [CrossRef]
10. Kleykamp, H. Enthalpy, Heat Capacity and Enthalpy of Transformation of Li_2TiO_3. *J. Nucl. Mater.* **2001**, *295*, 244–248. [CrossRef]
11. Tomiha, M.; Masaki, N.; Uchida, S.; Sato, T. Hydrothermal Synthesis of Alkali Titanates from Nano Size Titania Powder. *J. Mater. Sci.* **2002**, *37*, 2341–2344. [CrossRef]
12. Song, H.; Jiang, H.; Liu, T.; Liu, X.; Meng, G. Preparation and Photocatalytic Activity of Alkali Titanate Nano Materials $A_2Ti_nO_{2n+1}$ (A = Li, Na and K). *Mater. Res. Bull.* **2007**, *42*, 334–344. [CrossRef]
13. Laumann, A.; Fehr, K.T.; Wachsmann, M.; Holzapfel, M.; Iversen, B.B. Metastable Formation of Low Temperature Cubic Li_2TiO_3 under Hydrothermal Conditions—Its Stability and Structural Properties. *Solid State Ionics* **2010**, *181*, 1525–1529. [CrossRef]
14. Laumann, A.; Ørnsbjerg Jensen, K.M.; Tyrsted, C.; Bremholm, M.; Fehr, K.T.; Holzapfel, M.; Iversen, B.B. In-Situ Synchrotron X-Ray Diffraction Study of the Formation of Cubic Li_2TiO_3 Under Hydrothermal Conditions. *Eur. J. Inorg. Chem.* **2011**, *2011*, 2221–2226. [CrossRef]
15. Laumann, A.; Fehr, K.T.; Boysen, H.; Hölzel, M.; Holzapfel, M. Temperature-Dependent Structural Transformations of Hydrothermally Synthesized Cubic Li_2TiO_3 Studied by in-Situ Neutron Diffraction. *Zeitschrift für Kristallographie Crystalline Materials* **2011**, *226*, 53–61. [CrossRef]
16. Brandstätter, H.; Wohlmuth, D.; Bottke, P.; Pregartner, V.; Wilkening, M. Li Ion Dynamics in Nanocrystalline and Structurally Disordered Li_2TiO_3. *Z. Phys. Chem.* **2015**, *229*, 1363–1374. [CrossRef]
17. Carbajal-Ramos, I.A.; Andrade-Gamboa, J.J.; Condó, A.M.; Gennari, F.C. Formation of Cubic Li_2TiO_3 by Mechanical Activation and Its Transformation to Monoclinic Phase: Stability in Helium and Hydrogen Flows. *Solid State Ionics* **2017**, *308*, 46–53. [CrossRef]
18. Iwaniak, W.; Fritzsche, J.; Zukalová, M.; Winter, R.; Wilkening, M.; Heitjans, P. Li Conductivity of Nanocrystalline $Li_4Ti_5O_{12}$ Prepared by a Sol-Gel Method and High-Energy Ball Milling. *Defect Diffus. Forum* **2009**, *289–292*, 565–570. [CrossRef]
19. Becker, D.; Haberkorn, R.; Kickelbick, G. Mechanochemical Synthesis of Cubic Li_2TiO_3. *Zeitschrift für Kristallographie Supplements* **2017**, *37*, P178.
20. Indris, S.; Amade, R.; Heitjans, P.; Finger, M.; Haeger, A.; Hesse, D.; Grünert, W.; Börger, A.; Becker, K.D. Preparation by High-Energy Milling, Characterization, and Catalytic Properties of Nanocrystalline TiO_2. *J. Phys. Chem. B* **2005**, *109*, 23274–23278. [CrossRef] [PubMed]
21. Obrovac, M. Structure and Electrochemistry of $LiMO_2$ (M = Ti, Mn, Fe, Co, Ni) Prepared by Mechanochemical Synthesis. *Solid State Ionics* **1998**, *112*, 9–19. [CrossRef]
22. Jiang, K.; Hu, X.; Sun, H.; Wang, D.; Jin, X.; Ren, Y.; Chen, G.Z. Electrochemical Synthesis of $LiTiO_2$ and $LiTi_2O_4$ in Molten LiCl. *Chem. Mater.* **2004**, *16*, 4324–4329. [CrossRef]
23. Betke, A.; Kickelbick, G. Important Reaction Parameters in the Synthesis of Phenylphosphonic Acid Functionalized Titania Particles by Reactive Milling. *New J. Chem.* **2014**, *38*, 1264–1270. [CrossRef]
24. Gajovic, A.; Furic, K.; Music, S.; Djerdj, I.; Tonejc, A.; Tonejc, A.M.; Su, D.; Schlogl, R. Mechanism of $ZrTiO_4$ Synthesis by Mechanochemical Processing of TiO_2 and ZrO_2. *J. Am. Ceram. Soc.* **2006**, *89*, 2196–2205. [CrossRef]

25. Vijayakumar, M.; Kerisit, S.; Yang, Z.; Graff, G.L.; Liu, J.; Sears, J.A.; Burton, S.D.; Rosso, K.M.; Hu, J. Combined ^{6,7}Li NMR and Molecular Dynamics Study of Li Diffusion in Li_2TiO_3. *J. Phys. Chem. C* **2009**, *113*, 20108–20116. [CrossRef]
26. Baklanova, Y.V.; Arapova, I.Y.; Shein, I.R.; Maksimova, L.G.; Mikhalev, K.N.; Denisova, T.A. Charge Distribution and Mobility of Lithium Ions in Li_2TiO_3 from ^{6,7}Li NMR Data. *J. Struct. Chem.* **2013**, *54* (Suppl. 1), 111–118. [CrossRef]
27. Xu, Z.; Stebbins, J.F. 6Li Nuclear Magnetic Resonance Chemical Shifts, Coordination Number and Relaxation in Crystalline and Glassy Silicates. *Solid State Nucl. Magn. Reson.* **1995**, *5*, 103–112. [CrossRef]
28. Kartha, J.P.; Tunstall, D.P.; Irvine, J.T.S. An NMR Investigation of Lithium Occupancy of Different Sites in the Oxide Superconductor $LiTi_2O_4$ and Related Compounds. *J. Solid State Chem.* **2000**, *152*, 397–402. [CrossRef]
29. Leonidov, I.A.; Leonidova, O.N.; Perelyaeva, L.A.; Samigullina, R.F.; Kovyazina, S.A.; Patrakeev, M.V. Structure, Ionic Conduction, and Phase Transformations in Lithium Titanate $Li_4Ti_5O_{12}$. *Phys. Solid State* **2003**, *45*, 2183–2188. [CrossRef]
30. Bruker, A.X.; Topas, V. *General Profile and Structure Analysis Software for Powder Diffraction Data*; Bruker AXS: Karlsruhe, Germany, 2009.
31. Cheary, R.W.; Coelho, A.A.; Cline, J.P. Fundamental Parameters Line Profile Fitting in Laboratory Diffractometers. *J. Res. Natl. Inst. Stand. Technol.* **2004**, *109*, 1–25. [CrossRef] [PubMed]
32. Gražulis, S.; Chateigner, D.; Downs, R.T.; Yokochi, A.F.T.; Quirós, M.; Lutterotti, L.; Manakova, E.; Butkus, J.; Moeck, P.; Le Bail, A. Crystallography Open Database — An Open-Access Collection of Crystal Structures. *J. Appl. Crystallogr.* **2009**, *42*, 726–729. [CrossRef] [PubMed]
33. Lüke, H. *HPLueke Version 2—A Program for Running an HP 4192A Impedance Analyzer*; Marl, Germany, 2016.
34. Tarakina, N.V.; Neder, R.B.; Denisova, T.A.; Maksimova, L.G.; Baklanova, Y.V.; Tyutyunnik, A.P.; Zubkov, V.G. Defect Crystal Structure of New $TiO(OH)_2$ Hydroxide and Related Lithium Salt Li_2TiO_3. *Dalton Trans.* **2010**, *39*, 8168. [CrossRef] [PubMed]
35. Beck, H.P.; Douiheche, M.; Haberkorn, R.; Kohlmann, H. Synthesis and Characterisation of Chloro-Vanadato-Apatites $M_5(VO_4)_3Cl$ (M = Ca, Sr, Ba). *Solid State Sci.* **2006**, *8*, 64–70. [CrossRef]
36. Haberkorn, R.; Bauer, J.; Kickelbick, G. Chemical Sodiation of V_2O_5 by Na_2S. *Z. Anorg. Allg. Chem.* **2014**, *640*, 3197–3202. [CrossRef]

© 2018 by the authors. Licensee MDPI, Basel, Switzerland. This article is an open access article distributed under the terms and conditions of the Creative Commons Attribution (CC BY) license (http://creativecommons.org/licenses/by/4.0/).